

# Towards Black-Box Membership Inference Attack for Diffusion Models

Jingwei Li<sup>1,3</sup>, Jing Dong<sup>2</sup>, Tianxing He<sup>1,3</sup>, and Jingzhao Zhang<sup>1,3</sup>

<sup>1</sup>IIS, Tsinghua University

<sup>2</sup>The Chinese University of Hong Kong

<sup>3</sup>Shanghai Qizhi Institute

## Abstract

Given the rising popularity of AI-generated art and the associated copyright concerns, identifying whether an artwork was used to train a diffusion model is an important research topic. The work approaches this problem from the membership inference attack (MIA) perspective. We first identify the limitation of applying existing MIA methods for proprietary diffusion models: the required access of internal U-nets. To address the above problem, we introduce a novel membership inference attack method that uses only the image-to-image variation API and operates without access to the model’s internal U-net. Our method is based on the intuition that the model can more easily obtain an unbiased noise prediction estimate for images from the training set. By applying the API multiple times to the target image, averaging the outputs, and comparing the result to the original image, our approach can classify whether a sample was part of the training set. We validate our method using DDIM and Stable Diffusion setups and further extend both our approach and existing algorithms to the Diffusion Transformer architecture. Our experimental results consistently outperform previous methods.

## 1 Introduction

Recently, there has been a surge in the popularity of generative models, with diffusion models in particular, gaining huge attention within the AI community [42, 45, 46]. These models have demonstrated remarkable capabilities across various tasks, including unconditional image generation [14, 44], text-to-image generation [31, 36, 53] and image-to-image generation [37]. This surge has given rise to powerful AI art models such as DALL-E 2 [35], Stable Diffusion [36], and Imagen [38]. AI-generated art holds a promising future and is expected to have a widespread impact.

Effective training of diffusion models requires high-quality data. It is thus crucial to design an algorithm that can identify whether a specific artwork has been used during the training of a model, thereby providing protection for these artworks and detecting misuse of data. This is especially important due to the rapid growth of generative models, which has raised concerns over intellectual property (IP) rights, data privacy, and the ethical implications of training on copyrighted or proprietary content without consent. As these models are increasingly deployed across industries, detecting whether a specific piece of content was used in training can help prevent unauthorized use of artistic works, protecting creators’ copyrights and ownership rights. This is a classic problem in the field of machine learning, first introduced by [41] and named “membership inference attack”.

A series of studies have been conducted on membership inference attacks against diffusion models. [16] was the first to examine this issue, utilizing the loss function values of diffusion models to determine whether an image is in the training set. [6] and [20] extended this work by relaxing the assumptions about model access requirements.

Despite great progress, previous methods are not yet ready for MIA in proprietary diffusion models. Most existing approaches heavily rely on checking whether the U-net of the model predicts noise accurately, which is not practical since most commercial diffusion models available today offer only API access, while the U-net remains hidden.

To address the above issue, we propose a membership inference attack method that relies on the variation API and does not require access to the denoise model (e.g., U-net). We observe that if we alter an image using the target diffusion model’s variation API, the sampling process will be captured by “a region of attraction” if the model has seen this image during training (illustrated in Figure 2). Based on the above observation, we propose the REDIFFUSE algorithm for MIA with image-to-image variation API, and can detect member images without accessing the denoise model. Our main contributions are listed as follows:

1. We propose a membership inference attack method that **does not require access to the model’s internal structure**. Our method only involves using the model’s variation API to alter an image and compare it with the original one. We name our method REDIFFUSE.
2. We evaluate our method using DDIM [44] and Stable Diffusion [36] models on classical datasets, including CIFAR10/100 [22], STL10-Unlabeled [2], LAION-5B [40], etc. Our method outperforms the previous methods.
3. We extend both existing algorithms and our own algorithm to the Diffusion Transformer [33] architecture, implementing the membership inference attack within this model framework **for the first time**. Experimental results demonstrate that our algorithm is consistently effective.

## 2 Related Works

**Diffusion Model** The diffusion model, initially proposed by [42], has achieved remarkable results in producing high-quality samples across a variety of domains. This ranges from image generation [4, 45, 46], audio synthesis [17, 21, 34], and video generation [13, 15, 50], etc. Among existing diffusion models, the Denoising Diffusion Probabilistic Model (DDPM) [14] is one of the most frequently adopted. This approach introduces a dual-phase process for image generation: initially, a forward process gradually transforms training data into pure noise, followed by a reverse process that meticulously reconstructs the original data from this noise. Building on this model, there have been numerous follow-up studies, such as Stable Diffusion [36], which compresses images into a latent space and generates images based on text, and the Denoising Diffusion Implicit Models (DDIM) [44], which removes Gaussian randomness to accelerate the sampling generation process. These advancements demonstrate the versatility and potential of diffusion models.

**Data Safety and Membership Inference Attack** In the era of big data, preserving data privacy is paramount. The training of diffusion models may involve sensitive datasets like artists’ artworks, which are protected by copyright laws. Membership inference attacks, initially introduced by [41], serve as an effective means to detect potential misuse of data without proper authorization.

Its objective is to ascertain whether a particular data sample participated in the training phase of a target model. This approach is instrumental in probing privacy breaches and identifying illicit data utilization. Researchers primarily focus on membership inference attacks for classification models [24, 26, 39, 52], embedding models [7, 28, 43], and generative models [1, 10, 12].

In the domain of membership inference attacks against diffusion models, [16, 51] use a white-box approach, which assumes access to the entire diffusion model and utilizes loss and likelihood to determine whether a sample is in the training set. [6, 20, 47] have relaxed these requirements, eliminating the need for the entire model. They leverage the insight that samples within the training set yield more accurate noise predictions, thereby achieving high accuracy in membership inference attack tasks. However, they also require the outputs of the U-net, as it is necessary to obtain the noise predictions of intermediate steps. Recently, [32] proposed a black-box membership inference attack method against diffusion models. Their method identifies whether a specific image is in a finetuning dataset of 100 images by calculating the difference between the generated image and the target image, using the corresponding prompt as input. Their approach leverages the model’s tendency to memorize finetuning images and generate similar outputs. In contrast, we focus on detecting whether an image is in the pretraining dataset, where a pre-trained model often produces diverse outputs for the same prompt, making detection more challenging.

### 3 Preliminary

In this section, we begin by introducing the notations used for several popular diffusion models. We first introduce the Denoising Diffusion Probabilistic Model (DDPM) [14]. Then, we extend to the Denoising Diffusion Implicit Model (DDIM) [44] and Stable Diffusion [36], which are variants of DDPM used to accelerate image generation or generate images grounded in text descriptions. Lastly, we discuss Diffusion Transformer [33], a model that replaces the U-net architecture with a transformer and achieves higher-quality image generation.

**Denoising Diffusion Probabilistic Model (DDPM)** A diffusion model provides a stochastic path between an image and noise. The forward process (denoted as  $q$ ) iteratively incorporates Gaussian noise into an image, while the reverse process (denoted as  $p_\theta$ ) gradually reconstructs the image from noise.

$$\begin{aligned} q(x_t | x_{t-1}) &= \mathcal{N}\left(x_t; \sqrt{1 - \beta_t}x_{t-1}, \beta_t \mathbf{I}\right), \\ p_\theta(x_{t-1} | x_t) &= \mathcal{N}\left(x_{t-1}; \mu_\theta(x_t, t), \Sigma_\theta(x_t, t)\right), \end{aligned}$$

where  $\mu_\theta(\cdot)$  and  $\Sigma_\theta(\cdot)$  are the mean and covariance of the denoised image parameterized by the model parameters  $\theta$ , and  $\beta_t$  is a noise schedule that controls the amount of noise added at each step.

**Denoising Diffusion Implicit Model (DDIM)** DDIM modifies the sampling process to improve efficiency while maintaining high-quality image generation. Unlike DDPM, which requires a large number of denoising steps, DDIM uses a non-Markovian process to accelerate sampling.

$$x_{t-1} = \phi_\theta(x_t, t) = \sqrt{\bar{\alpha}_{t-1}} \left( \frac{x_t - \sqrt{1 - \bar{\alpha}_t} \epsilon_\theta(x_t, t)}{\sqrt{\bar{\alpha}_t}} \right) + \sqrt{1 - \bar{\alpha}_{t-1}} \epsilon_\theta(x_t, t), \quad (1)$$

where  $\bar{\alpha}_t = \prod_{k=0}^t \alpha_k$ ,  $\alpha_t + \beta_t = 1$  and  $\epsilon_\theta(x_t, t)$  is the noise predicted by the model at step  $t$ . This formulation requires fewer sampling steps without compromising the quality of the generated images.

**Stable Diffusion** Stable Diffusion leverages a variational autoencoder (VAE) [19] to encode images into a latent space and perform diffusion in this compressed space. The model uses a text encoder to guide the diffusion process, enabling text-to-image generation:

$$z_{t-1} \sim p_{\theta}(z_{t-1} | z_t, \tau_{\theta}(y)), \quad x = \text{Decoder}(z_0),$$

where  $x$  represents the output image,  $z_t$  represents the latent variable at step  $t$ , and the text conditioning  $\tau_{\theta}(y)$  is incorporated into the denoising process to generate the image. This approach significantly reduces computational costs and allows for high-quality image synthesis from textual descriptions.

**Diffusion Transformer** Diffusion Transformer leverages the Vision Transformer [5] structure to replace the U-net architecture traditionally used in diffusion models for noise prediction. Its training and sampling methods remain consistent with DDIM, with the only difference being the replacement of noise prediction network  $\epsilon_{\theta}$  with  $\epsilon_{\tilde{\theta}}$ , where  $\tilde{\theta}$  represents a Vision Transformer-based architecture. This approach further enhances the generation quality and ensured that the model possesses good scalability properties.

## 4 Algorithm Design

In this section, we introduce our algorithm. We begin by discussing the definition of variation API and the limitations of previous membership inference attack methods. In our formulations, we assume DDIM as our target model. The formulations for DDPM are highly similar and we omit it for brevity. We will discuss the generalization to the latent diffusion model in Section 4.3.

### 4.1 The variation API for Diffusion Models

Most previous works on membership inference attacks against diffusion models aim to prevent data leakage and hence rely on thresholding the model’s training loss. For instance, [16] involves a direct comparison of image losses, while [6, 20] evaluates the accuracy of the model’s noise prediction at initial or intermediate steps. However, the required access to the model’s internal U-net structure prevents applications from copyright protection because most servers typically provide only black-box API access.

In contrast, our method represents a step towards black-box MIA, as we do not directly access the model’s internal structure. Instead, we rely solely on the variation API, which takes an input image and returns the corresponding output image. Below, we formalize the definition of the variation API used in our algorithm.

**Definition 1** (The variation API). We define the variation API  $V_{\theta}(x, t)$  of a model as follows. Suppose we have an input image  $x$ , and the diffusion step of the API is  $t$ . The variation API randomly adds  $t$ -step Gaussian noise  $\epsilon \sim \mathcal{N}(0, I)$  to the image and denoises it using the DDIM sampling process  $\phi_{\theta}(x_t, t)$  as described in Equation 1, returning the reconstructed image  $V_{\theta}(x, t) = \hat{x}$ . The details are as follows:

$$x_t = \sqrt{\bar{\alpha}_t}x + \sqrt{1 - \bar{\alpha}_t}\epsilon, \quad \hat{x} = \Phi_{\theta}(x_t, 0) = \phi_{\theta}(\cdots \phi_{\theta}(\phi_{\theta}(x_t, t), t - 1), 0). \quad (2)$$

This definition aligns with the image-to-image generation method of the diffusion model, making access to this API practical in many setups [27, 37, 49]. Some APIs provide the user with a choice

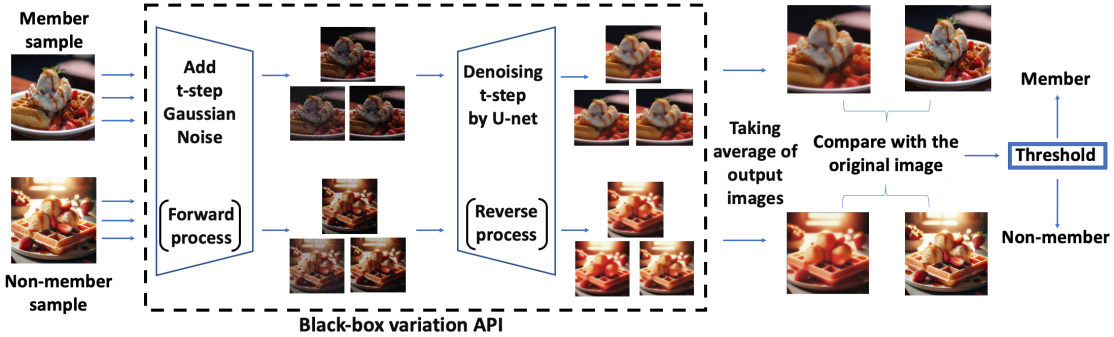


**Figure 1: The overview of REDIFFUSE.** We independently input the image to the variation API  $n$  times with diffusion step  $t$ . We take the average of the output images and compare them with the original ones. If the difference is below a certain threshold, we determine that the image is in the training set.

of  $t$ , while others do not and use the default parameter. We will discuss the influence of different diffusion steps in Section 5.5, showing that the attack performances are relatively stable and not sensitive to the selection of  $t$ . We also note that for the target model, we can substitute  $\phi_\theta(x_t, 0)$  with other sampling methods, such as the Euler-Maruyama Method [29] or Variational Diffusion Models [18].

## 4.2 Algorithm

In this section, we present the intuition of our algorithm. We denote  $\|\cdot\|$  as the  $L_2$  operator norm of a vector and  $\mathcal{T} = \{1, 2, \dots, T\}$  as the set of diffusion steps. The key insight is derived from the training loss function of a fixed sample  $x_0$  and a time step  $t \in \mathcal{T}$ :

$$L(\theta) = \mathbb{E}_{\epsilon \sim \mathcal{N}(0, \mathbf{I})} \left[ \left\| \epsilon - \epsilon_\theta \left( \sqrt{\bar{\alpha}_t} x_0 + \sqrt{1 - \bar{\alpha}_t} \epsilon, t \right) \right\|^2 \right].$$

Denote  $x_t = \sqrt{\bar{\alpha}_t} x_0 + \sqrt{1 - \bar{\alpha}_t} \epsilon$ , we assume that the denoise model is expressive enough such that for the input  $x_0 \in \mathbb{R}^d$  and time step  $t \in \mathcal{T}$ , the Jacobian matrix  $\nabla_{\theta} \epsilon_\theta(x_t, t)$  is full rank ( $\geq d$ ). This suggest that the model can adjust the predicted noise  $\epsilon_\theta(x_t, t)$  locally in any direction. Then for a well trained model, we would have

$$\begin{aligned} \nabla_{\theta} L(\theta) = 0 &\implies \nabla_{\theta} \epsilon_\theta(x_t, t)^T \mathbb{E}_{\epsilon \sim \mathcal{N}(0, \mathbf{I})} \left[ \epsilon - \epsilon_\theta \left( \sqrt{\bar{\alpha}_t} x_0 + \sqrt{1 - \bar{\alpha}_t} \epsilon, t \right) \right] = 0, \\ &\implies \mathbb{E}_{\epsilon \sim \mathcal{N}(0, \mathbf{I})} \left[ \epsilon - \epsilon_\theta \left( \sqrt{\bar{\alpha}_t} x_0 + \sqrt{1 - \bar{\alpha}_t} \epsilon, t \right) \right] = 0. \end{aligned}$$

Intuitively, this is because if the noise prediction from the neural network exhibited high bias, the network could adjust to fit the bias term, further reducing the training loss.

Therefore, for images in the training set, we expect the network to provide an unbiased noise prediction. Since the noise prediction is typically inaccessible in practical applications, we use the reconstructed sample  $\hat{x}$  as a proxy. Leveraging the unbiasedness of noise prediction, we demonstrate that averaging over multiple independent reconstructed samples  $\hat{x}_i$  significantly reduces estimation error (see Theorem 1). On the other hand, for images that are not in the training set, the neural network may not provide an unbiased prediction at these points. We illustrate the intuition in Figure 2.

With the above intuition, we introduce the details of our algorithm. We independently apply the variation API  $n$  times with our target image  $x$  as input, average the output images, and then

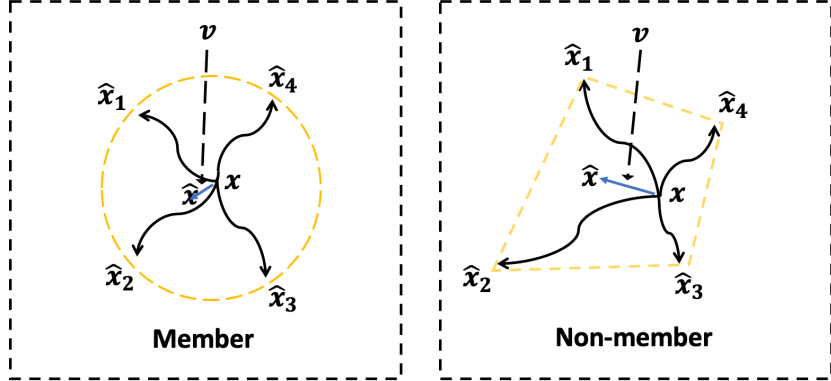


**Figure 2: The intuition of our algorithm design.** We denote  $x$  as the target image,  $\hat{x}_i$  as the  $i$ -th image generated by the variation API, and  $\hat{x}$  as the average image of them. For member image  $x$ , the difference  $v = x - \hat{x}$  will be smaller after averaging due to  $x_i$  being an unbiased estimator.

compare the average result  $\hat{x}$  with the original image. We will discuss the impact of the averaging number  $n$  in Section 5.5. We then evaluate the difference between the images using an indicator function:

$$f(x) = \mathbf{1}[D(x, \hat{x}) < \tau].$$

Our algorithm classifies a sample as being in the training set if  $D(x, \hat{x})$  is smaller than a threshold  $\tau$ , where  $D(x, \hat{x})$  represents the difference between the two images. It can be calculated using traditional functions, such as the SSIM metric [48]. Alternatively, we can train a neural network as a proxy. In Section 5, we will introduce the details of  $D(x, \hat{x})$  used in our experiment.

Our algorithm is outlined in Algorithm 1, and we name it REDIFFUSE. The key ideas of our algorithm are illustrated in Figure 1, and we also provide some theoretical analysis in Theorem 1 to support it.

---

**Algorithm 1** MIA through REDIFFUSE

---

**Input:** Target image  $x$ , diffusion step  $t$ , average number  $n$ , threshold  $\tau$ , the variation API of the target model  $V_\theta$ , distance function  $D$ .

**for**  $k = 1, \dots, n$  **do**

Use the variation API  $V_\theta$  to generate the variation image  $\hat{x}_k = V_\theta(x, t)$  according to Equation (2).

**end for**

Average the reconstructed images from each iteration  $\hat{x} = \frac{1}{n}(\hat{x}_1 + \hat{x}_2 + \dots + \hat{x}_n)$ .

**return** "YES" if the distance between the two images  $D(x, \hat{x})$  is less than  $\tau$ , otherwise "NO".

---

**Analysis** We give a short analysis to justify why averaging over  $n$  samples in REDIFFUSE can reduce the prediction error for training data. We have the following theorem showing that if we use the variation API to input a member  $x \sim D_{\text{training}}$ , then the error  $\|\hat{x} - x\|$  from our method will be small with high probability.

**Theorem 1.** *Suppose the DDIM model can learn a parameter  $\theta$  such that, for any  $x \sim D_{\text{training}}$  with dimension  $d$ , the prediction error  $\epsilon - \epsilon_\theta(\sqrt{\bar{\alpha}_t}x + \sqrt{1 - \bar{\alpha}_t}\epsilon, t)$  is a random variable  $X = (X_1, X_2, \dots, X_d)$  with zero expectation and finite cumulant-generating function for each coordinate [8]. Suppose the sampling interval  $k$  is equal to the variation API diffusion step  $t$ . Let  $\hat{x}$  be the average of  $n$  output images of  $x$  using the variation API. Then we have*

$$\mathbb{P}(\|\hat{x} - x\| \geq \beta) \leq d \exp \left( -n \min_i \Psi_{X_i}^* \left( \frac{\beta \sqrt{\bar{\alpha}_t}}{\sqrt{d(1 - \bar{\alpha}_t)}} \right) \right),$$

where  $\beta > 0$  and  $\Psi_{X_i}^*$  is the Fenchel-Legendre dual of the cumulant-generating function  $\Psi_{X_i}$ .

The theorem suggests that averaging the randomly variational data from a training set will result in a smaller relative error with high probability when we use a large  $n$ . We defer the proof of this theorem to Appendix C.

We note that the unbiased assumption on predicted noise can be strong in practice. For experiments, we expect the mean  $\|\mu\|$  of predicted noise for trained data is smaller than the mean  $\|\mu'\|$  from unseen data. As a result, the empirical best choice of  $n$  would be determined by the gap  $\|\mu'\| - \|\mu\|$ .

### 4.3 MIA on Other Diffusion Models

In this section, we discuss how we can generalize our algorithm to other diffusion models. We note that the variation API for stable diffusion is different from DDIM, as it includes the encoder-decoder process. Again we denote  $\hat{x} = V_\theta(x, t)$ , and the details are as follows:

$$z = \text{Encoder}(x), \quad z_t = \sqrt{\bar{\alpha}_t}z + \sqrt{1 - \bar{\alpha}_t}\epsilon, \quad \hat{z} = \Phi_\theta(z_t, 0), \quad \hat{x} = \text{Decoder}(\hat{z}). \quad (3)$$

This definition aligns with the image generation process of the stable diffusion model.

For the Diffusion Transformer, we define the variation API as  $V_{\tilde{\theta}}(x, t)$ , where  $\tilde{\theta}$  corresponds to the Vision Transformer architecture instead of the U-net. We repeatedly call the variation API and calculate the difference between the original image and the reconstructed image, as done in DDIM.

## 5 Experiments

In this section, we evaluate the performance of our methods across various datasets and settings. We follow the same experiment setup in previous papers [6, 20]. The detailed experimental settings, including datasets, models, and hyper-parameter settings can be found in Appendix A.

### 5.1 Evaluation Metrics

We follow the metrics used in previous papers [6, 20], including Area Under Receiver Operating Characteristic (AUC), Attack Success Rate (ASR), the True Positive Rate (TP) when the False Positive Rate is 1%. We also plot the ROC curves.

### 5.2 MIA with DDIM Models

We follow the experimental setup of [6, 20]. We train a DDIM model on the CIFAR-10/100 [22] and STL10-Unlabeled datasets [2], using the image generation step  $T = 1000$  and sampling interval  $k = 100$ . For all the datasets, we randomly select 50% of the training samples to train the model and denote them as members. The remaining 50% are utilized as nonmembers. We use [30], [6], [20] as

our baseline methods. We fix the diffusion step at  $t = 200$ , and independently call the variation API 10 times to take the average of the output images as  $\hat{x}$ . We will discuss the impact of the diffusion step and the average number in Section 5.5.

**Table 1:** Comparison of different methods on four datasets for the DDIM model. We use AUC, ASR, and TP as the metrics, TP refers to the True Positive Rate when the False Positive Rate is 1%.

Method		CIFAR10			CIFAR100			STL10		
Algorithm	U-Net	AUC	ASR	TP	AUC	ASR	TP	AUC	ASR	TP
Loss [30]	□	0.88	0.82	14.2	0.92	0.84	20.9	0.89	0.82	15.6
SecMI [6]	□	0.95	0.90	40.7	0.96	0.90	44.9	0.94	0.88	26.9
PIA [20]	□	0.95	0.89	48.7	0.96	0.90	47.0	0.94	0.87	29.8
PIAN [20]	□	0.95	0.89	<b>50.4</b>	0.91	0.85	39.2	0.92	0.86	28.5
<b>REDIFFUSE</b>	■	<b>0.96</b>	<b>0.91</b>	40.7	<b>0.98</b>	<b>0.93</b>	<b>48.2</b>	<b>0.96</b>	<b>0.90</b>	<b>31.9</b>

□: Require the access of U-Net. ■: Do not require the access of U-Net.

For the difference function  $D(x, \hat{x})$ , following the setup in [6], we take the pixel-wise absolute value of  $x - \hat{x}$  to obtain a difference vector  $v$  for each image. Using the ResNet-18 network [11] and denoting it as  $f_R$ , we perform binary classification on these difference vectors. We use 20% of the data as the training set and obtained the label of each difference vector being classified as a member or nonmember. The difference function is obtained by the negated value of the probability outputted by the neural network predicting as member:  $D(x, \hat{x}) = -f_R(v)$ .

The result is shown in Table 1. Our method achieves high performance, surpassing several baseline algorithms in most setups, and does not require access to the internal structure of the model. This demonstrates that our algorithm is highly effective and robust.

### 5.3 MIA with Diffusion Transformers

We train a diffusion transformer model on the ImageNet [3] dataset following the setup of [33]. We randomly select 100,000 images from the ImageNet training set to train the model with resolutions of either  $128 \times 128$  or  $256 \times 256$ . For the membership inference attack setup, 1000 images are randomly chosen from our training set as the member set, and another 1000 images are randomly selected from the ImageNet validation set as the non-member set. We fix the diffusion step at  $t = 150$  and the DDIM step at  $k = 50$ , and independently call the variation API 10 times to take the average of the output images as  $\hat{x}$ .

We use [30], [6], [20] as our baseline methods. Since these work did not study the case of Diffusion Transformers, we integrate their algorithms into the DiT framework for evaluation. For the difference function  $D(x, \hat{x})$ , following the setup in [6, 20], we take the L2 norm of  $x - \hat{x}$  to measure the differences between two image. The results, presented in Table 2, demonstrate that our method outperforms baseline algorithms and does not require access to the Vision Transformer.

We also plot ROC curves for the DDIM train on CIFAR-10 and the Diffusion Transformer train on ImageNet  $256 \times 256$  in Figure 3. The curves further demonstrate the effectiveness of our method.



**Table 2:** Comparison of different methods for Diffusion Transformer using the same set of metrics as Table 1. Previous methods require access to the Vision Transformer, whereas our methods do not. We use AUC, ASR, and TP as the metrics, TP refers to the True Positive Rate when the False Positive Rate is 1%.

Method		ImageNet 128 × 128			ImageNet 256 × 256		
Algorithm	Transformer	AUC	ASR	TP	AUC	ASR	TP
Loss [30]	□	0.83	0.76	10.7	0.78	0.70	7.3
SecMI [6]	□	0.80	0.73	8.3	0.88	0.80	16.3
PIA [20]	□	0.97	0.92	32.1	0.91	0.85	6.8
PIAN [20]	□	0.66	0.64	6.2	0.67	0.66	12.8
<b>REDIFFUSE</b>	■	<b>0.98</b>	<b>0.95</b>	<b>44.1</b>	<b>0.97</b>	<b>0.94</b>	<b>47.3</b>

□: Require the access of Transformer. ■: Do not require the access of Transformer.

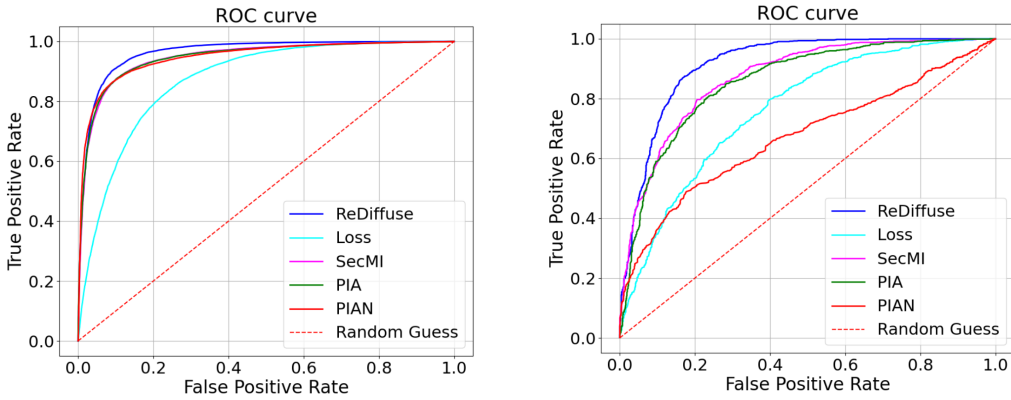


**Figure 3: The ROC curves of various setups.** Left: DDIM model on CIFAR-10. Right: Diffusion Transformer on ImageNet 256 × 256. The curves show that our algorithm outperforms the baseline algorithms.

#### 5.4 MIA with the Stable Diffusion Model

We conduct experiments on the original Stable Diffusion model, i.e., stable-diffusion-v1-4 provided by Huggingface, without further fine-tuning or modifications. We follow the experiment setup of [6, 20], use the LAION-5B dataset [40] as member and COCO2017-val [25] as non-member. We randomly select 2500 images in each dataset. We test two scenarios: Knowing the ground truth text, which we denote as Laion5; Not knowing the ground truth text and generating text through BLIP [23], which we denote as Laion5 with BLIP.

For the difference function  $D(x, \hat{x})$ , since the images in these datasets better correlate with human visual perception, we directly use the SSIM metric [48] to measure the differences between two images. The results, presented in Table 3, demonstrate that our methods achieve high accuracy in this setup, outperforming baseline algorithms by approximately 10%. Notably, our methods do not require access to U-Net.

**Table 3:** Comparison of different methods for Stable Diffusion using the same set of metrics as Table 1. Again, previous methods require access to U-Net, whereas our methods do not. We use AUC, ASR and TP as the metrics, TP refers to the True Positive Rate when the False Positive Rate is 1%.

Method		Laion5			Laion5 with BLIP		
Algorithm	U-Net	AUC	ASR	TP	AUC	ASR	TP
Loss [30]	□	0.62	0.61	13.2	0.62	0.62	13.3
SecMI [6]	□	0.70	0.65	19.2	0.71	0.66	19.8
PIA [20]	□	0.70	0.66	19.7	0.73	0.68	20.2
PIAN [20]	□	0.56	0.53	4.8	0.55	0.51	4.4
<b>ReDIFFUSE</b>	■	<b>0.81</b>	<b>0.75</b>	<b>20.6</b>	<b>0.82</b>	<b>0.75</b>	<b>21.7</b>

□: Require the access of U-Net. ■: Do not require the access of U-Net.

## 5.5 Ablation Studies

In this section, we alter some experimental parameters to test the robustness of our algorithm. We primarily focus on the ablation study of DDIM and Diffusion Transformer, while the ablation study related to Stable Diffusion is provided in Appendix B.

**The Impact of Average Numbers** We test the effect of using different averaging numbers  $n$  on the results, as shown in Figure 4. It can be observed that averaging the images from multiple independent samples to generate the output  $\hat{x}$  further improves accuracy. This observation validates the algorithm design intuition discussed in Section 4.2. Additional figures showing the ASR results are presented in Appendix B.

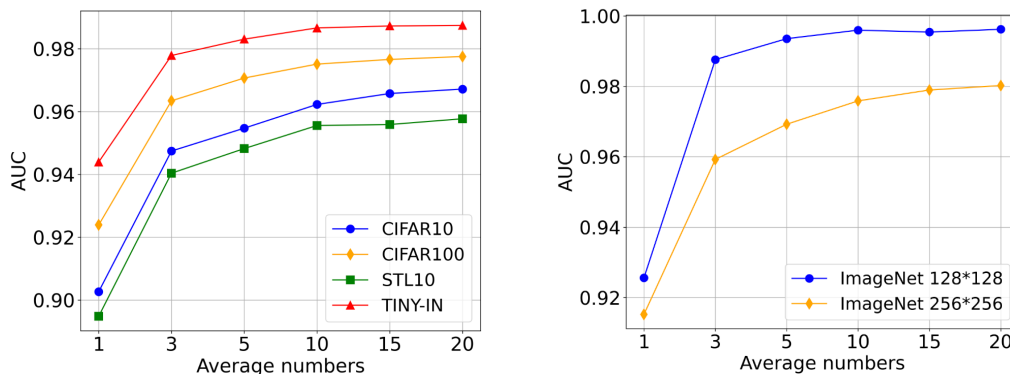


**Figure 4: The impact of average numbers.** Left: DDIM model on CIFAR-10. Right: Diffusion Transformer model on Imagenet. In both cases, averaging multiple independent samples proves to be effective in further improving the overall performance of our algorithm, which validates the intuition of our algorithm design.

**The Impact of Diffusion Steps** We adjust the diffusion step  $t$  to examine its impact on the results. The experiments are conducted using the DDIM model on CIFAR-10 with diffusion steps for

inference. The outcomes are presented in Figure 5. Our findings indicate that as long as a moderate step is chosen, the attack performance remains excellent, demonstrating that our algorithm is not sensitive to the choice of  $t$ . This further underscores the robustness of our algorithm. We also plot the change of diffusion step for other diffusion models and datasets in the Appendix B.

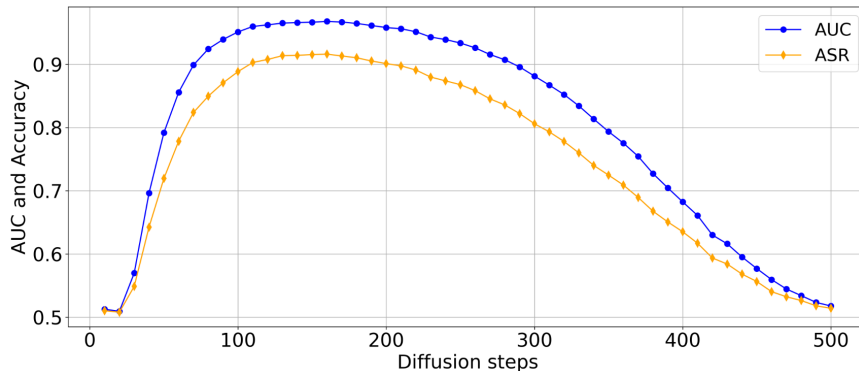


**Figure 5: The impact of diffusion steps on DDIM.** We train a DDIM model on the CIFAR-10 dataset and use different diffusion steps for inference. We find that high accuracy can be achieved as long as a moderate step number is chosen. This opens up possibilities for practical applications in real-world scenarios.

**The Impact of Sampling Intervals** In DDIM and Diffusion Transformer, the model uses a set of steps denoted by  $\tau_1, \tau_2, \dots, \tau_T$ . It samples each of these steps to create the image. The spacing between these steps is referred to as the sampling interval. We change the sampling interval  $k$  and check the influence on the results. As shown in Figure 6, we adjust this parameter for attacks on both DDIM and Diffusion Transformer. We find that our method achieves high AUC values across different sampling intervals, demonstrating that our detection capabilities are not significantly limited by this parameter. Additionally, in Appendix B, we plot the effect of different sampling intervals on ASR and find that the impact is minimal.

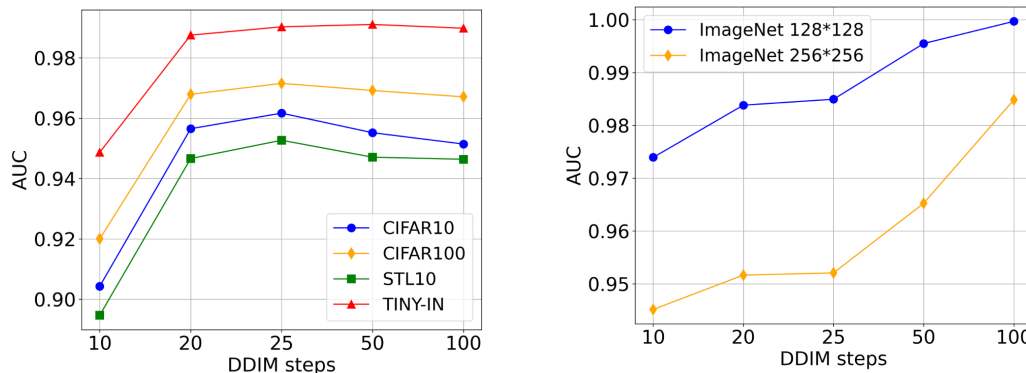


**Figure 6: The impact of sampling intervals.** Left: DDIM model on CIFAR-10. Right: Stable Diffusion model on LAION-5. We find that adjusting the sampling interval has a relatively small influence in the first case and does not affect our method in the latter case. This makes our algorithm applicable to more setups.

## 6 An Application to DALL-E’s API

In this section, we conduct a small experiment with online API services to test the effectiveness of our algorithm. We test with the DALL-E 2 [35] model since DALL-E 2 provides a variation API service.

We select different thresholds and classify an image with a variation error below the threshold as members and those above the threshold as non-members. We then calculate metrics such as AUC and ASR. Since the baseline algorithms [6, 20, 30] require intermediate results, we are unable to test these algorithms under the online API setup.

One challenge with MIA for DALL-E 2 is that it does not disclose its training set. However, since it is adept at generating various famous artworks, we select 30 famous paintings from five famous artists: Van Gogh, Monet, Da Vinci, Dali, and Rembrandt, to form our member set. We believe that it is reasonable to hypothesize that these artworks are used in DALL-E 2’s training set. For constructing the non-member set, we used Stable Diffusion 3 [9] to generate images based on the titles of each painting in the member set. The benefit of constructing non-members in this way is that it allows for control over the content of the artwork descriptions, reducing bias caused by content shift. Moreover, these generated images are certainly not in the DALL-E 2’s training set. Other results of changes to the member and non-member inputs after applying the variation API can be found in Appendix D.

The results, presented in Table 4, demonstrate that our algorithm achieves a relatively high accuracy under this evaluation method. Our observation is illustrated in Figure 17. As seen in the figure, for Monet’s iconic painting "Water Lily Pond", the original artwork shows minimal changes when using DALL-E 2’s variation API, retaining most of its main features. In contrast, the artwork generated by Stable Diffusion 3 undergoes significant changes, with variations in both the number of flowers and lily pads. Therefore, we hypothesize that artworks with smaller changes after API usage are more likely to have appeared in the model’s training set.

**Table 4: The results of applying our algorithm to DALL-E 2’s variation API.** We assume some famous paintings as members and use Stable Diffusion 3 along with the titles of these artworks to generate corresponding non-members. Our algorithm also achieves high accuracy under this setup. Since the baseline algorithm requires noise prediction results, we are unable to evaluate it in this black-box setup.

Metrics	$L_1$ distance	$L_2$ distance
AUC	76.2	88.3
ASR	74.5	81.4

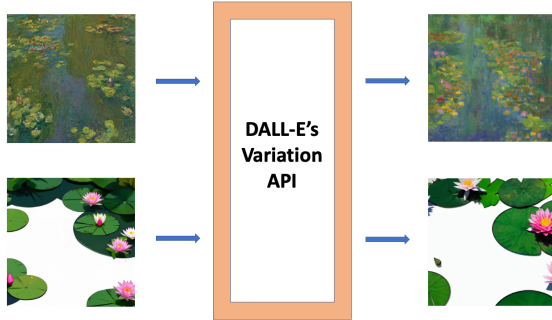


**Figure 7: Main observation of our attack.** DALL-E 2’s variation API makes minimal changes to famous artworks, while nonmember images with similar content undergo significant alterations.

The results indicate that we can apply our algorithm with online API services. We acknowledge that this part of the experimental design has certain limitations. Not every famous painting we selected may be present in DALL-E 2’s training set, and our construction of non-members may exhibit some distribution shift relative to the member dataset. Here, we aim to provide a real-world

application for black-box evaluation, leaving a more comprehensive experimental design as future work.

## 7 Conclusion, Limitations and Future Directions

In this work, we introduce a novel membership inference attack method specifically designed for diffusion models. Our approach only requires access to the variation API of the model, bypassing the need for internal network components such as the U-net. This represents an advancement for commercial diffusion models, which typically restrict internal access. We demonstrate the effectiveness of our approach across various datasets, showing that it achieves high accuracy in identifying whether an image was included in the training dataset. Our algorithm can detect data misuse by the model, representing a step forward in protecting the copyright of artworks.

However, our method has certain limitations, particularly the requirement for a moderate diffusion step  $t$  in the variation API. The algorithm’s accuracy declines when the diffusion step is excessively high. As such, we propose our method as an initial step towards black-box MIA, with a more comprehensive solution left for subsequent exploration.

Future work could focus on developing more robust algorithms capable of handling a broader range of diffusion steps. Improving the interpretability of our method and extending it to other generative models are also valuable directions for further research.

## References

- [1] Dingfan Chen, Ning Yu, Yang Zhang, and Mario Fritz. Gan-leaks: A taxonomy of membership inference attacks against generative models. In *Proceedings of the 2020 ACM SIGSAC conference on computer and communications security*, pages 343–362, 2020.
- [2] Adam Coates, Andrew Ng, and Honglak Lee. An analysis of single-layer networks in unsupervised feature learning. In *Proceedings of the fourteenth international conference on artificial intelligence and statistics*, pages 215–223. JMLR Workshop and Conference Proceedings, 2011.
- [3] Jia Deng, Wei Dong, Richard Socher, Li-Jia Li, Kai Li, and Li Fei-Fei. Imagenet: A large-scale hierarchical image database. In *2009 IEEE conference on computer vision and pattern recognition*, pages 248–255. Ieee, 2009.
- [4] Prafulla Dhariwal and Alexander Nichol. Diffusion models beat gans on image synthesis. *Advances in neural information processing systems*, 34:8780–8794, 2021.
- [5] Alexey Dosovitskiy. An image is worth 16x16 words: Transformers for image recognition at scale. *arXiv preprint arXiv:2010.11929*, 2020.
- [6] Jinhao Duan, Fei Kong, Shiqi Wang, Xiaoshuang Shi, and Kaidi Xu. Are diffusion models vulnerable to membership inference attacks? In *International Conference on Machine Learning*, pages 8717–8730. PMLR, 2023.
- [7] Vasisht Duddu, Antoine Boutet, and Virat Shejwalkar. Quantifying privacy leakage in graph embedding. In *MobiQuitous 2020-17th EAI International Conference on Mobile and Ubiquitous Systems: Computing, Networking and Services*, pages 76–85, 2020.

- [8] R Durrett. Probability, theory and examples, cambride ser. *Stat. and Prob. Math., Cambridge University Press, New York*, page 65, 2010.
- [9] Patrick Esser, Sumith Kulal, Andreas Blattmann, Rahim Entezari, Jonas Müller, Harry Saini, Yam Levi, Dominik Lorenz, Axel Sauer, Frederic Boesel, et al. Scaling rectified flow transformers for high-resolution image synthesis. In *Forty-first International Conference on Machine Learning*, 2024.
- [10] Jamie Hayes, Luca Melis, George Danezis, and Emiliano De Cristofaro. Logan: Membership inference attacks against generative models. *arXiv preprint arXiv:1705.07663*, 2017.
- [11] Kaiming He, Xiangyu Zhang, Shaoqing Ren, and Jian Sun. Deep residual learning for image recognition. In *Proceedings of the IEEE conference on computer vision and pattern recognition*, pages 770–778, 2016.
- [12] Benjamin Hilprecht, Martin Härterich, and Daniel Bernau. Monte carlo and reconstruction membership inference attacks against generative models. *Proceedings on Privacy Enhancing Technologies*, 2019.
- [13] Jonathan Ho, William Chan, Chitwan Saharia, Jay Whang, Ruiqi Gao, Alexey Gritsenko, Diederik P Kingma, Ben Poole, Mohammad Norouzi, David J Fleet, et al. Imagen video: High definition video generation with diffusion models. *arXiv preprint arXiv:2210.02303*, 2022.
- [14] Jonathan Ho, Ajay Jain, and Pieter Abbeel. Denoising diffusion probabilistic models. *Advances in neural information processing systems*, 33:6840–6851, 2020.
- [15] Jonathan Ho, Tim Salimans, Alexey Gritsenko, William Chan, Mohammad Norouzi, and David J Fleet. Video diffusion models. *Advances in Neural Information Processing Systems*, 35:8633–8646, 2022.
- [16] Hailong Hu and Jun Pang. Membership inference of diffusion models. *arXiv preprint arXiv:2301.09956*, 2023.
- [17] Rongjie Huang, Max WY Lam, Jun Wang, Dan Su, Dong Yu, Yi Ren, and Zhou Zhao. Fastdiff: A fast conditional diffusion model for high-quality speech synthesis. *arXiv preprint arXiv:2204.09934*, 2022.
- [18] Diederik Kingma, Tim Salimans, Ben Poole, and Jonathan Ho. Variational diffusion models. *Advances in neural information processing systems*, 34:21696–21707, 2021.
- [19] Diederik P Kingma and Max Welling. Auto-encoding variational bayes. *arXiv preprint arXiv:1312.6114*, 2013.
- [20] Fei Kong, Jinhao Duan, RuiPeng Ma, Hengtao Shen, Xiaofeng Zhu, Xiaoshuang Shi, and Kaidi Xu. An efficient membership inference attack for the diffusion model by proximal initialization. *arXiv preprint arXiv:2305.18355*, 2023.
- [21] Zhifeng Kong, Wei Ping, Jiaji Huang, Kexin Zhao, and Bryan Catanzaro. Diffwave: A versatile diffusion model for audio synthesis. *arXiv preprint arXiv:2009.09761*, 2020.

- [22] Alex Krizhevsky, Geoffrey Hinton, et al. Learning multiple layers of features from tiny images. 2009.
- [23] Junnan Li, Dongxu Li, Caiming Xiong, and Steven Hoi. Blip: Bootstrapping language-image pre-training for unified vision-language understanding and generation. In *International conference on machine learning*, pages 12888–12900. PMLR, 2022.
- [24] Zheng Li and Yang Zhang. Membership leakage in label-only exposures. In *Proceedings of the 2021 ACM SIGSAC Conference on Computer and Communications Security*, pages 880–895, 2021.
- [25] Tsung-Yi Lin, Michael Maire, Serge Belongie, James Hays, Pietro Perona, Deva Ramanan, Piotr Dollár, and C Lawrence Zitnick. Microsoft coco: Common objects in context. In *Computer Vision–ECCV 2014: 13th European Conference, Zurich, Switzerland, September 6–12, 2014, Proceedings, Part V 13*, pages 740–755. Springer, 2014.
- [26] Yunhui Long, Vincent Bindschaedler, Lei Wang, Diyue Bu, Xiaofeng Wang, Haixu Tang, Carl A Gunter, and Kai Chen. Understanding membership inferences on well-generalized learning models. *arXiv preprint arXiv:1802.04889*, 2018.
- [27] Andreas Lugmayr, Martin Danelljan, Andres Romero, Fisher Yu, Radu Timofte, and Luc Van Gool. Repaint: Inpainting using denoising diffusion probabilistic models. In *Proceedings of the IEEE/CVF conference on computer vision and pattern recognition*, pages 11461–11471, 2022.
- [28] Saeed Mahloujifar, Huseyin A Inan, Melissa Chase, Esha Ghosh, and Marcello Hasegawa. Membership inference on word embedding and beyond. *arXiv preprint arXiv:2106.11384*, 2021.
- [29] Xuerong Mao. The truncated euler–maruyama method for stochastic differential equations. *Journal of Computational and Applied Mathematics*, 290:370–384, 2015.
- [30] Tomoya Matsumoto, Takayuki Miura, and Naoto Yanai. Membership inference attacks against diffusion models. In *2023 IEEE Security and Privacy Workshops (SPW)*, pages 77–83. IEEE, 2023.
- [31] Alex Nichol, Prafulla Dhariwal, Aditya Ramesh, Pranav Shyam, Pamela Mishkin, Bob McGrew, Ilya Sutskever, and Mark Chen. Glide: Towards photorealistic image generation and editing with text-guided diffusion models. *arXiv preprint arXiv:2112.10741*, 2021.
- [32] Yan Pang and Tianhao Wang. Black-box membership inference attacks against fine-tuned diffusion models. *arXiv preprint arXiv:2312.08207*, 2023.
- [33] William Peebles and Saining Xie. Scalable diffusion models with transformers. In *Proceedings of the IEEE/CVF International Conference on Computer Vision*, pages 4195–4205, 2023.
- [34] Vadim Popov, Ivan Vovk, Vladimir Gogoryan, Tasnima Sadekova, and Mikhail Kudinov. Grad-tts: A diffusion probabilistic model for text-to-speech. In *International Conference on Machine Learning*, pages 8599–8608. PMLR, 2021.

- [35] Aditya Ramesh, Prafulla Dhariwal, Alex Nichol, Casey Chu, and Mark Chen. Hierarchical text-conditional image generation with clip latents. *arXiv preprint arXiv:2204.06125*, 1(2):3, 2022.
- [36] Robin Rombach, Andreas Blattmann, Dominik Lorenz, Patrick Esser, and Björn Ommer. High-resolution image synthesis with latent diffusion models. In *Proceedings of the IEEE/CVF conference on computer vision and pattern recognition*, pages 10684–10695, 2022.
- [37] Chitwan Saharia, William Chan, Huiwen Chang, Chris Lee, Jonathan Ho, Tim Salimans, David Fleet, and Mohammad Norouzi. Palette: Image-to-image diffusion models. In *ACM SIGGRAPH 2022 conference proceedings*, pages 1–10, 2022.
- [38] Chitwan Saharia, William Chan, Saurabh Saxena, Lala Li, Jay Whang, Emily L Denton, Kamyar Ghasemipour, Raphael Gontijo Lopes, Burcu Karagol Ayan, Tim Salimans, et al. Photorealistic text-to-image diffusion models with deep language understanding. *Advances in neural information processing systems*, 35:36479–36494, 2022.
- [39] Ahmed Salem, Yang Zhang, Mathias Humbert, Pascal Berrang, Mario Fritz, and Michael Backes. MI-leaks: Model and data independent membership inference attacks and defenses on machine learning models. *arXiv preprint arXiv:1806.01246*, 2018.
- [40] Christoph Schuhmann, Romain Beaumont, Richard Vencu, Cade Gordon, Ross Wightman, Mehdi Cherti, Theo Coombes, Aarush Katta, Clayton Mullis, Mitchell Wortsman, et al. Laion-5b: An open large-scale dataset for training next generation image-text models. *Advances in Neural Information Processing Systems*, 35:25278–25294, 2022.
- [41] Reza Shokri, Marco Stronati, Congzheng Song, and Vitaly Shmatikov. Membership inference attacks against machine learning models. In *2017 IEEE symposium on security and privacy (SP)*, pages 3–18. IEEE, 2017.
- [42] Jascha Sohl-Dickstein, Eric Weiss, Niru Maheswaranathan, and Surya Ganguli. Deep unsupervised learning using nonequilibrium thermodynamics. In *International conference on machine learning*, pages 2256–2265. PMLR, 2015.
- [43] Congzheng Song and Ananth Raghunathan. Information leakage in embedding models. In *Proceedings of the 2020 ACM SIGSAC conference on computer and communications security*, pages 377–390, 2020.
- [44] Jiaming Song, Chenlin Meng, and Stefano Ermon. Denoising diffusion implicit models. *arXiv preprint arXiv:2010.02502*, 2020.
- [45] Yang Song and Stefano Ermon. Generative modeling by estimating gradients of the data distribution. *Advances in neural information processing systems*, 32, 2019.
- [46] Yang Song, Jascha Sohl-Dickstein, Diederik P Kingma, Abhishek Kumar, Stefano Ermon, and Ben Poole. Score-based generative modeling through stochastic differential equations. *arXiv preprint arXiv:2011.13456*, 2020.
- [47] Shuai Tang, Zhiwei Steven Wu, Sergul Aydore, Michael Kearns, and Aaron Roth. Membership inference attacks on diffusion models via quantile regression. *arXiv preprint arXiv:2312.05140*, 2023.



- [48] Zhou Wang, Alan C Bovik, Hamid R Sheikh, and Eero P Simoncelli. Image quality assessment: from error visibility to structural similarity. *IEEE transactions on image processing*, 13(4):600–612, 2004.
- [49] Chen Henry Wu and Fernando De la Torre. A latent space of stochastic diffusion models for zero-shot image editing and guidance. In *Proceedings of the IEEE/CVF International Conference on Computer Vision*, pages 7378–7387, 2023.
- [50] Jay Zhangjie Wu, Yixiao Ge, Xintao Wang, Stan Weixian Lei, Yuchao Gu, Yufei Shi, Wynne Hsu, Ying Shan, Xiaohu Qie, and Mike Zheng Shou. Tune-a-video: One-shot tuning of image diffusion models for text-to-video generation. In *Proceedings of the IEEE/CVF International Conference on Computer Vision*, pages 7623–7633, 2023.
- [51] Yixin Wu, Ning Yu, Zheng Li, Michael Backes, and Yang Zhang. Membership inference attacks against text-to-image generation models. *arXiv preprint arXiv:2210.00968*, 2022.
- [52] Samuel Yeom, Irene Giacomelli, Matt Fredrikson, and Somesh Jha. Privacy risk in machine learning: Analyzing the connection to overfitting. In *2018 IEEE 31st computer security foundations symposium (CSF)*, pages 268–282. IEEE, 2018.
- [53] Jiahui Yu, Yuanzhong Xu, Jing Yu Koh, Thang Luong, Gunjan Baid, Zirui Wang, Vijay Vasudevan, Alexander Ku, Yinfei Yang, Burcu Karagol Ayan, et al. Scaling autoregressive models for content-rich text-to-image generation. *arXiv preprint arXiv:2206.10789*, 2(3):5, 2022.

## A Datasets, Models and Hyperparameters

We use NVIDIA RTX 6000 graphics cards for all our experiments.

For DDIM, we follow the training hyperparameters of [6] to train a DDIM model on the CIFAR-10/100 [22] and STL10-Unlabeled [2] datasets, using 1000 image generation steps ( $T = 1000$ ) and a sampling interval of  $k = 100$ . The training iterations are set to 800,000. For all the datasets, we randomly select 50% of the training samples to train the model and designate them as members. The remaining 50% of the training samples are used as nonmembers.

We use [6, 20, 30] as our baseline methods. We use their official code repositories and apply the optimal hyperparameters from their papers. For our algorithm, we fix the diffusion step at  $t = 200$  and independently call the variation API 10 times to average the output images as  $\hat{x}$ .

For the Diffusion Transformers, we train the model on the ImageNet [3] dataset, using 1000 image generation steps ( $T = 1000$ ), while for other training hyperparameters, we follow the setup of [33]. We randomly select 100,000 images from the ImageNet training set to train the model at resolutions of either  $128 \times 128$  or  $256 \times 256$ . For the  $128 \times 128$  image size, we use 160,000 training iterations. For the  $256 \times 256$  image size, we use 300,000 training iterations. These numbers of training iterations are chosen to ensure the generation of high-quality images.

For the membership inference attack setup, 1000 images are randomly selected from our training set as the member set, and another 1000 images are randomly chosen from the ImageNet validation set as the non-member set. We fix the diffusion step at  $t = 150$  and the DDIM step at  $k = 50$ , and independently call the variation API 10 times to average the output images as  $\hat{x}$ .

We also use [6, 20, 30] as our baseline methods. Since these papers do not study Diffusion Transformers, we adapt their algorithms to the DiT framework for evaluation. We fix the DDIM step at  $k = 50$  and choose diffusion steps  $t \in [50, 100, 150, 200, 250, 300]$ , recording their optimal solutions under these different hyperparameter settings.

For the Stable Diffusion experiments, we use the original Stable Diffusion model, i.e., stable-diffusion-v1-4 provided by Huggingface, without further fine-tuning or modifications. We follow the experimental setup of [6, 20], using an image generation step of  $T = 1000$  and a sampling interval of  $k = 10$ . We use the LAION-5B dataset [40] as the member set and COCO2017-val [25] as the non-member set. We randomly select 2500 images from each dataset. We test two scenarios: knowing the ground truth text, denoted as Laion; and generating text through BLIP [23], denoted as Laion with BLIP.

We use the hyperparameters from the papers [6, 20] to run the baseline methods. For our algorithms REDIFFUSE, we fix the diffusion step at  $t = 10$  to call the variation API and directly use the SSIM metric [48] to measure the differences between two images. Other hyperparameters remain the same as in the baseline methods.

## B More Experiment Results

In this section, we show other experiment results which is not in our main paper. We conduct more ablation studies.

**The Impact of Average Numbers** We use different average numbers  $n$  and test the influence on the results. Besides the figures of AUC in the main paper, the figures of ASR of DDIM and Diffusion Transformer are also plotted in Figure 8. In addition, we plot the figures of AUC and ASR for Stable Diffusion in Figure 9. We observe that in the DDIM and Diffusion Transformer setup, averaging the images from multiple independent samples as the output further improves accuracy. In the stable diffusion setup, since the image size in the dataset is larger (512x512), the reconstructed images are more stable and not influenced by perturbations at specific coordinates. Therefore, averaging multiple images is not necessary.

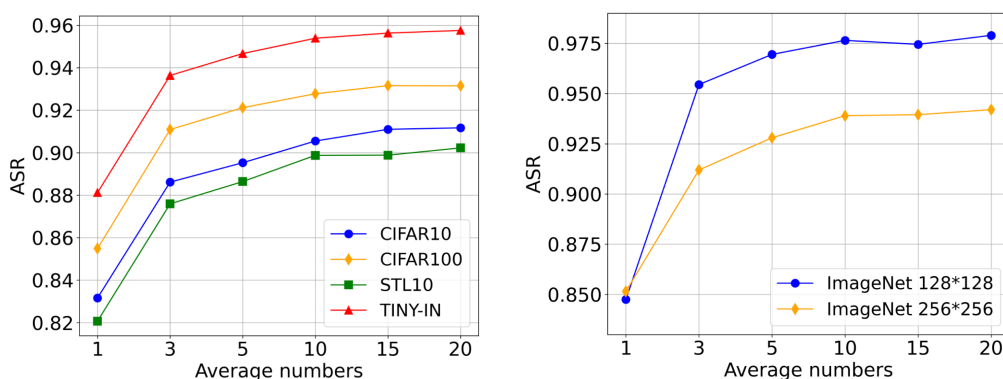


**Figure 8: The impact of average numbers.** Left: DDIM model on CIFAR-10. Right: Diffusion Transformer model on Imagenet. Averaging can further improve the performance of our algorithm.

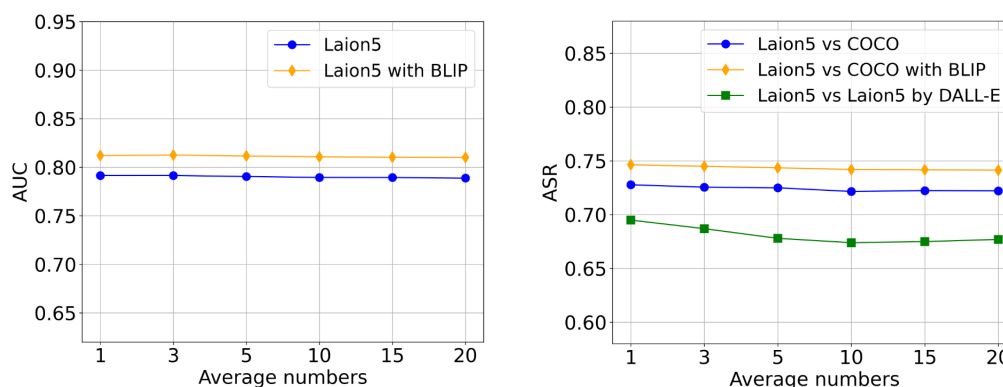


**Figure 9: The impact of average numbers on Stable Diffusion.** We plot the AUC and ASR metrics, and averaging does not improve performance.

**The Impact of Diffusion Steps** We adjust the diffusion step  $t$  to examine its impact on the results. We train the DDIM model on CIFAR100 (Figure 10), STL10 (Figure 11) dataset, Diffusion Transformer on the Imagenet  $256 \times 256$  (Figure 12) dataset and Stable Diffusion on Laion5 dataset (Figure 13). From the results, we see that our algorithm can achieve high performance over a wide range of diffusion steps. This opens up possibilities for practical applications in real-world scenarios.

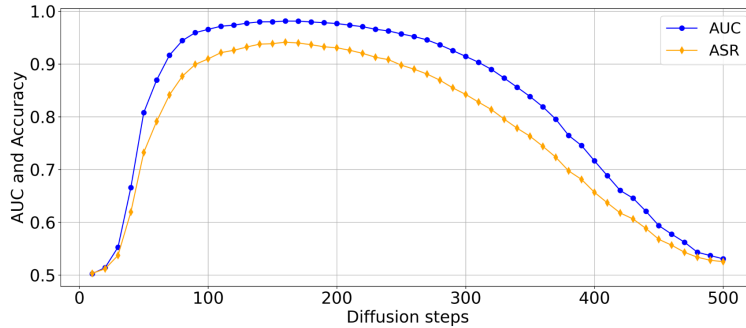


**Figure 10: The impact of diffusion steps.** We train a DDIM model on the CIFAR-100 dataset and use different diffusion step for inference.

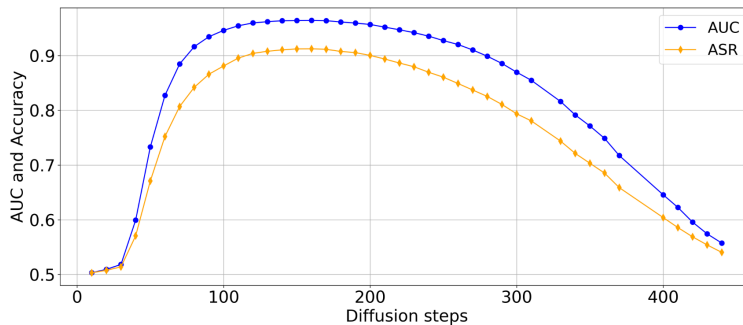


**Figure 11: The impact of diffusion steps.** We train a DDIM model on the STL-10 dataset and use different diffusion step for inference.

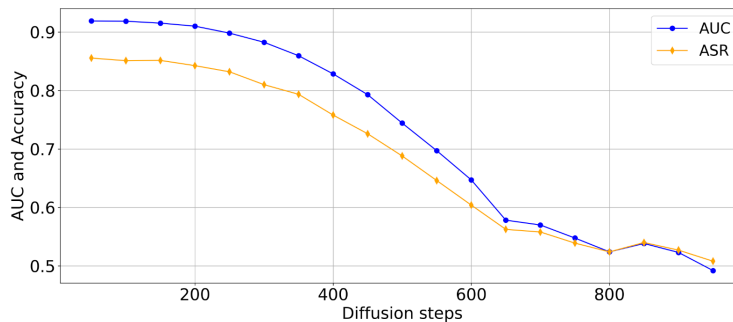


**Figure 12: The impact of diffusion steps.** We train a Diffusion Transformer model on the Imagenet  $256 \times 256$  dataset and use different diffusion step for inference. The robust results imply that our algorithm is also not very sensitive to the choice of  $t$  in this setup.

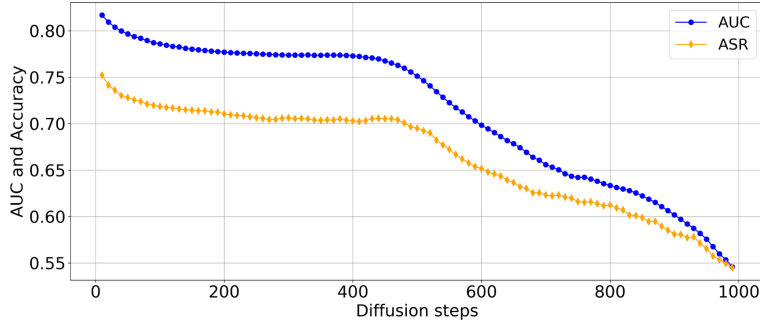


**Figure 13: The impact of diffusion steps.** We use the Stable Diffusion model with the Laion5 dataset for evaluation and test different diffusion steps for inference. Specifically, using relatively small diffusion steps results in better performance.

**The Impact of Sampling Intervals** We change the sampling intervals to see if there is any influence on the results. In addition to the AUC figures in the main paper, the ASR figures of DDIM and Diffusion Transformer are also plotted in Figure 14. We also plot the AUC and ASR for Stable Diffusion in Figure 15. From the results, we observe that our algorithm consistently performs well across different sampling intervals.

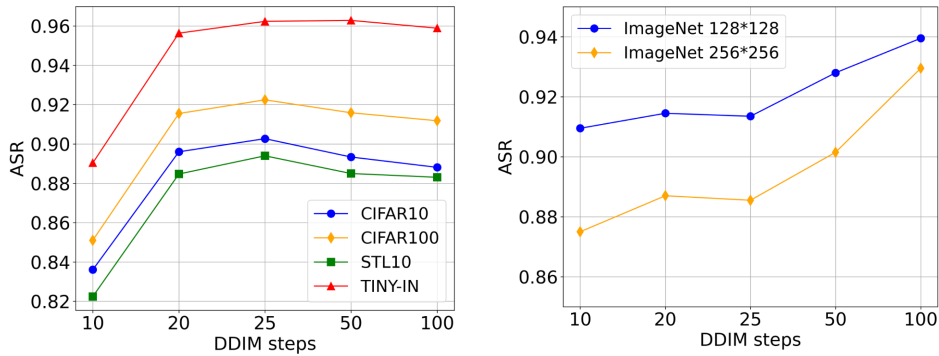


**Figure 14: The impact of sampling intervals.** Left: DDIM model on CIFAR-10. Right: Diffusion Transformer on Imagenet. We find that adjusting the sampling interval does not significantly affect of the accuracy.

**The ROC curves** Besides the ROC curves in the main paper, we also plot ROC curves for the Diffusion Transformer train on ImageNet  $128 \times 128$  and the Stable Diffusion train on Laion5 in Figure 16. The curves further demonstrate the effectiveness of our method.

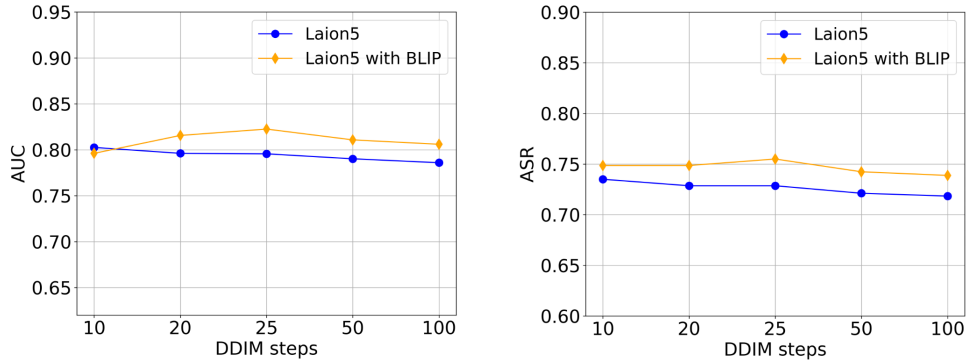


**Figure 15: The impact of sampling intervals on Stable Diffusion.** We plot the AUC and ASR metrics, observe that different sampling intervals have minimal impact on it.

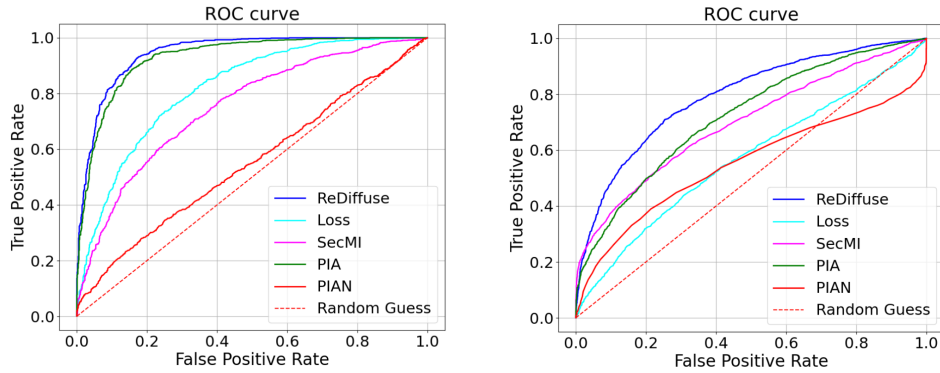


**Figure 16: The ROC curves of various setups.** Left: Diffusion Transformer on ImageNet  $128 \times 128$ . Right: The Stable Diffusion on Laion5. The curves show that our algorithm outperforms the baseline algorithms.

## C Proof

In this section, we implement the proof of the theorem.

**Theorem 1.** Suppose the DDIM model can learn a parameter  $\theta$  such that, for any  $x \sim D_{\text{training}}$  with dimension  $d$ , the prediction error  $\epsilon - \epsilon_{\theta}(\sqrt{\bar{\alpha}_t}x + \sqrt{1 - \bar{\alpha}_t}\epsilon, t)$  is a random variable  $X = (X_1, X_2, \dots, X_d)$  with zero expectation and finite cumulant-generating function for each coordinate [8]. Suppose the sampling interval  $k$  is equal to the variation API diffusion step  $t$ . Let  $\hat{x}$  be the average of  $n$  output images of  $x$  using the variation API. Then we have

$$\mathbb{P}(\|\hat{x} - x\| \geq \beta) \leq d \exp \left( -n \min_i \Psi_{X_i}^* \left( \frac{\beta \sqrt{\bar{\alpha}_t}}{\sqrt{d(1 - \bar{\alpha}_t)}} \right) \right),$$

where  $\beta > 0$  and  $\Psi_{X_i}^*$  is the Fenchel-Legendre dual of the cumulant-generating function  $\Psi_{X_i}$ .

*Proof.* We denote  $x^i$  as the  $i$ -th output image of  $x$  using the variation API. We denote the  $i$ -th Gaussian noise as  $\epsilon^i$  and the forward process incur  $x_t^i = \sqrt{\bar{\alpha}_t}x + \sqrt{1 - \bar{\alpha}_t}\epsilon^i$ .

As the sampling interval is equal to the variation API diffusion step  $t$ , we have

$$\begin{aligned}
x^i - x &= \frac{x_t^i - \sqrt{1 - \bar{\alpha}_t} \epsilon_\theta(\sqrt{\bar{\alpha}_t} x + \sqrt{1 - \bar{\alpha}_t} \epsilon^i, t)}{\sqrt{\bar{\alpha}_t}} - x, \\
&= \frac{\sqrt{\bar{\alpha}_t} x + \sqrt{1 - \bar{\alpha}_t} \epsilon^i - \sqrt{1 - \bar{\alpha}_t} \epsilon_\theta(\sqrt{\bar{\alpha}_t} x + \sqrt{1 - \bar{\alpha}_t} \epsilon^i, t)}{\sqrt{\bar{\alpha}_t}} - x, \\
&= \frac{\sqrt{1 - \bar{\alpha}_t}}{\sqrt{\bar{\alpha}_t}} (\epsilon^i - \epsilon_\theta(\sqrt{\bar{\alpha}_t} x + \sqrt{1 - \bar{\alpha}_t} \epsilon^i, t)).
\end{aligned}$$

If we denote the random variable  $X^i = (X_1^i, X_2^i, \dots, X_d^i)$  represents  $\epsilon^i - \epsilon_\theta(\sqrt{\bar{\alpha}_t} x + \sqrt{1 - \bar{\alpha}_t} \epsilon^i, t)$ , then we consider  $S_n^i = \sum_{j=1}^n X_j^i$ . From the assumption we know that all the  $X_j^i$  are random variables with zero expectation and finite cumulant-generating function  $\Psi_X(s) = \log E[e^{sX}] < +\infty$ . Using the theorem of Chernoff-Cramer method for sums of IID RV [8], we get the following probability inequality for any  $\beta > 0$ :

$$\mathbb{P}(|S_n^i| \geq \beta) \leq \exp(-n \Psi_{X^i}^*(\frac{\beta}{n})),$$

where  $\beta > 0$  and  $\Psi_X^*(y) = \sup_{s>0} (sy - \Psi_X(s))$  is the Fenchel-Legendre dual of the cumulant-generating function  $\Psi_X$ .

Therefore, denote  $S_n = (S_n^1, S_n^2, \dots, S_n^d)$ , taking the definition of  $\|\hat{x} - x\| = \|\frac{1}{n} \sum_{i=1}^n (x^i - x)\| = \frac{\sqrt{1 - \bar{\alpha}_t}}{n\sqrt{\bar{\alpha}_t}} \|S_n\|$ , we get the following bound of the reconstruction error:

$$\mathbb{P}(\|\hat{x} - x\| \geq \beta) \leq \sum_{i=1}^d P(|S_n^i| \geq \frac{n\beta\sqrt{\bar{\alpha}_t}}{\sqrt{d(1 - \bar{\alpha}_t)}}) \leq d \exp(-n \min_i \Psi_{X^i}^*(\frac{\beta\sqrt{\bar{\alpha}_t}}{\sqrt{d(1 - \bar{\alpha}_t)}})),$$

So averaging the randomly reconstructed data from a training set will result in a smaller reconstruction error with high probability of  $\Theta(1 - \exp(-n))$  when we use a large  $n$ .

□

## D More Results of Variation Images

In this section, we provide more results of the variation of member and nonmember image when applying to DALL-E 2's variation API. The experimental results are recorded in Figure 17, from which we can see that the variation in the member inputs after applying the DALL-E 2's variation API is relatively small than non-member inputs.

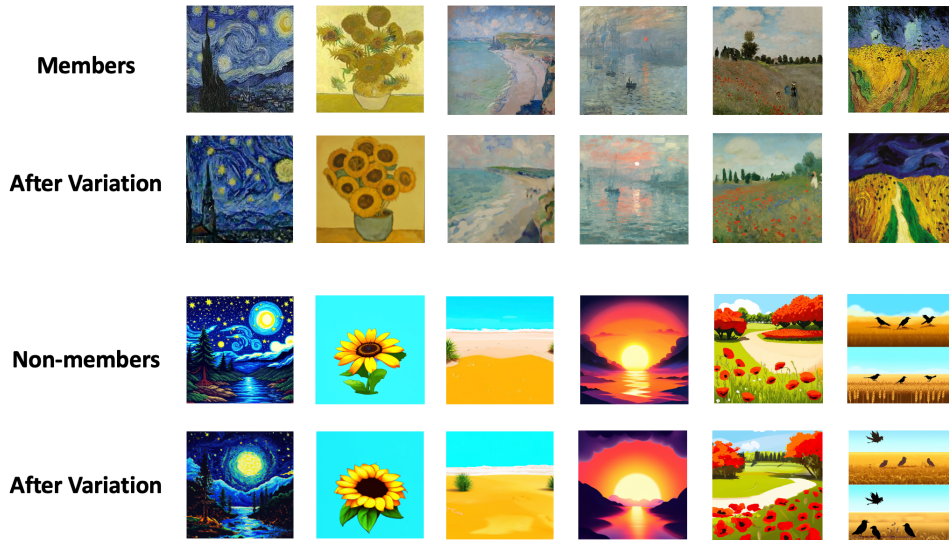


**Figure 17: More results of the variation images.** From the figures we can see that DALL-E 2's variation API makes less changes to images in member set than non-member set.